UiO : Department of Geosciences
University of Oslo

Direct Solution for Closed f/H Contour Dynamics in High Latitude Ocean Basins

Magnus Dyrmose Ryseth
Master's Thesis, Autumn 2022

Sammendrag

En lineær modell, utviklet fra gruntvannsteori, evnet å kvalitativt gjenskape sirkulasjonen til en kompleks og høyoppløst havmodell om lukkede f/H-konturer ved høye breddegrader. De eneste variablene den lineære modellen tok inn var topp- og bunnstress. Kun den lineære bunnfriksjonsparameteren inngår som ukjent i den lineære modellen. For hver f/H-kontur i studien, ble en serie av verdier for bunnstressparameteren testet mot havmodellen, og den som genererte høyest korrelasjon mellom de to modellene ble valgt. Sammenlikninger mellom resultatene for havmodellen og den lineære modellen er presentert innenfor tre rammeverk. Først ble tidsseriene til begge modeller tegnet for hver kontur og sammenliknet direkte. Så ble det utført koherensestimater for å undersøke på hvilke tidsskalaer de to modellene harmonerer. Til sist ble spredningsgrafer tegnet for å undersøke ved hvilke numeriske verdier den lineære modellen fungerer best. Ytelsen til den lineære modellen, i form av lineær korrelasjon, ligger på verdier rundt $0.8 - 0.9$ for bassenger i de nordiske hav, og når verdier over 0.8 for de største konturene i bassenger i Nordishavet. Basert på koherens presterte den lineære modellen best på tidsskalaer lengre enn omkring 5 til 10 dager. En av oppdagelsene i studien var at den lineære modellen presterte signifikant bedre for syklonisk strømning enn for antisyklonisk strømning. De middelmådige resultatene for antisyklonisk strømning ble tilskrevet en velkjent asymmetri mellom prograd og retrograd bevegelse, grunnet ikkelineær instabilitet. En utvidelse av teorien, med turbulente laterale virvlingsflukser, ga ingen merkbare forbedringer i dens prestasjon. Dog ble det funnet en minimumshastighet for konturfølgende strømning på omkring 2.5 cm/s, grunnet effektene av virvlingsflukser. Den lineære modellen er valid for strømning som er raskere enn dette.

Abstract

A linear model, developed from shallow-water theory, was able to qualitatively reproduce the circulation about closed high-latitude f/H-contours, of a complex high-resolution ocean model, only using surface and bottom stress components as input. The sole unknown in the linear model is the linear bottom friction parameter. For each studied f/H-contour, a range of values for bottom stress was tested, and the one yielding the highest correlation between the two models was picked. Comparisons between the results of the ocean model and linear model are presented in three frameworks. First, the time series of both models were plotted for every contour, and compared. Secondly, coherence estimates were made to investigate at which time-scales the two models harmonise. Thirdly, scatter plots of the two models were examined to investigate at which values the linear model performs best. The performance of the linear model, in terms of linear correlation, lies in the range $0.8-0.9$ for the basins of the Nordic Seas, and reaches values above 0.8 for the largest contours of the Arctic Ocean basins. Viewing coherence, the linear model performed best on time scales of more than approximately ten days. It was found that the linear model performed significantly better for cyclonic motion, than for anticyclonic motion. The mediocre results in anticyclonic modes were ascribed to a well-known asymmetry in prograde and retrograde flow, caused by nonlinear instability. An expansion of the theory, with eddy lateral vorticity fluxes, yielded no noticeable improvements on its performance. However, a flux contribution assessment found that the linear model is valid only for along-contour velocities above approximately 2.5 cm/s, due to the effect of the fluxes.

Acknowledgements

This thesis has been in the works for more than a year, and along the way I've learned much about the ocean and myself - as well as worked with, and around, people who have made the experience a very good one.

I want to thank my supervisors, Pål Erik Isachsen and Joe LaCasce, who, during my first semester at UiO, aided in awaking my interest for the ocean, and who hinted at this annoyance in the Eurasian Basin that had been gnawing in the back of their minds for almost 20 years.
Specifically, I want to thank Pål Erik, who consistently inspired me to try new approaches, and motivated me through periods where models didn't want to cooperate, and my belief in the project and myself was declining. It seems to have worked out in the end, so thanks for helping me stay focused! I also want to thank Joe for sharing his extensive knowledge of the physics of the ocean with me, and for always keeping me on my toes.

Karen, my oceanography partner in crime, deserves some big thanks for all the talks and discussions we've shared, both before exams and during the writing of our theses. I would also like to thank Anna Lina for all the chats and help (even though you weren't allowed to help).

To the gang at Lesesal 2418B: thanks so much for the fantastic time we've shared! Coming to Oslo during Covid-19 would have been very different for me if it hadn't been for all of you. We'll keep in touch.

Finally, I would like to give thanks to my family and close friends, for always supporting me and showing genuine interest in my work. You have all been the absolute best, tusen takk!

Oslo, May 2022
Magnus Dyrmose Ryseth

Contents

List of Figures

List of Tables

CHAPTER 1

Introduction

In the changing climate of Earth, the Arctic has experienced the greatest mean temperature increase, a phenomenon known as Arctic amplification (Previdi et al., 2021). This is the case both for the atmosphere and the ocean, and, as such, the Arctic system is greatly unbalanced. The effects of heating are changing atmospheric dynamics, with a pole-ward shift of storms and weaker thermal wind. Additionally, the multi-year sea-ice of the Arctic Ocean is diminishing, and the waters may be completely ice free in summers within the next few decades (Haine and Martin, 2017). Within the ocean, Arctic amplification weakens the density gradient between low and high latitudes, along with the freshening of the high latitudes ocean due to ice-sheet and glacier mass loss. This could have severe impacts on the Atlantic meridional overturning circulation, effectively weakening it (Boers, 2021). While the system struggles to reach a new equilibrium state due to the continuous thermal forcing of heightened atmospheric greenhouse gas concentrations, it remains in unbalance (Timmermans and Marshall, 2020).

The Earth system is complicated and interconnected within different spheres (Eyring et al., 2016), and is therefore challenging to model and understand. Climate models incorporate routines for the atmosphere, ocean and sea-ice, which in turn may have hundreds of variables that interact in a nonlinear manner and have different feedback cycles. It is of general interest to understand the dynamic mechanisms of the system, in order to facilitate accurate predictions for the change and increase model quality. Identification of the governing factors of the climate system could aid in performing efficient, targeted, studies. Doing calculations with these factors exclusively could produce reliable results for the dynamics in the system without running demanding and complex coupled models.

The primary motivation for this project, perhaps, is that identification of dominant forcers increases the intuitive knowledge about drivers of the system, which to some extent can be lost when solely viewing complex models. This thesis explores ocean dynamics for the high latitudes of the Northern hemisphere, utilising a high resolution ocean model. Results from simplified theory are compared the output of the model.

1.1 Study area

The Nordic Seas and Arctic Ocean are characterised by five major deep ocean basins. These are the Norwegian and Greenland Basins of the Nordic Seas, and the Eurasian, Makarov and Canadian Basins of the Arctic Ocean. The region of study is displayed in figure 1.1. Regarding sea-ice, the waters covering the Norwegian Basin are constantly ice free, while the Greenland Basin has some ice coverage in the North-West, with a maximum in winter. The basins of the Arctic Ocean are fully covered in winter, and are mostly covered during summer (Stroeve et al., 2011). Additionally, the sea-ice is thicker in winter, and a large portion of it is bound to land as fast ice, rendering it immobile. Summer ice is thinner, more broken up and less bound to land, increasing its mobility. The seasonal difference in ice-cover impacts the air-sea fluxes, also momentum fluxes. The Nordic Seas experience frequent cyclonic storms that enter from the South-West (Brayshaw et al., 2011), most often in autumn and winter. The Arctic Weather is calmer, and a persistent high pressure system (the Beaufort high) oftentimes lies above the Canadian Basin waters (Serreze and Barrett, 2011).

Bathymetric steering of the large-scale oceanic motion is a phenomenon of the high latitudes seas that has long been recognised, and was first described by Helland-Hansen and Nansen (1909). Their observations can be ascribed to the ocean bathymetry via the quantity f/H. Here f accounts for the Coriolis parameter, or planetary vorticity, and H is the ocean depth. At high latitudes, f varies little and ,thus, bathymetry dominates the quantity. To conserve potential vorticity, large scale ocean currents follow contours of constant f/H.

The North-Atlantic Current moves water along open f/H-contours on the Norwegian Continental Shelf, and enters the Arctic through the Fram Strait and the Barents Sea (e.g. Aagard et al., 1987). Water exits the Arctic along the shelf East of Greenland and through the Canadian Archipelago. Thus, there is a consistent cyclonic motion along the f/H-contours that are open to the North Atlantic. Using the familiar Sverdrup balance, developed for the sub-tropics, is insufficient for the Nordic Seas and Arctic Ocean, due to the absence of blocked f/H-contours.

The basins mentioned above have closed f/H-contours, where the large-scale flow also tends to follow the contours in a recirculating manner. The dynamics of these closed contours, shown as black lines in figure 1.1, will be studied in this thesis.

1.2 Hypotheses

The wind-driven variability of recirculating flows in high latitude ocean basins was investigated by Isachsen et al. (2003). With linear theory, they managed to successfully describe the motion cohesively for up to about five years in the Nordic Seas and Canadian basins. However, the results for the Eurasian Basin were poorer. For this project three main hypotheses for how to more successfully describe the dynamics of the basins were introduced. The first hypothesis is that Isachsen et al. (2003) used a too simple surface stress parameterisation over ice-covered regions, and that a more complex parameterisation could yield a better

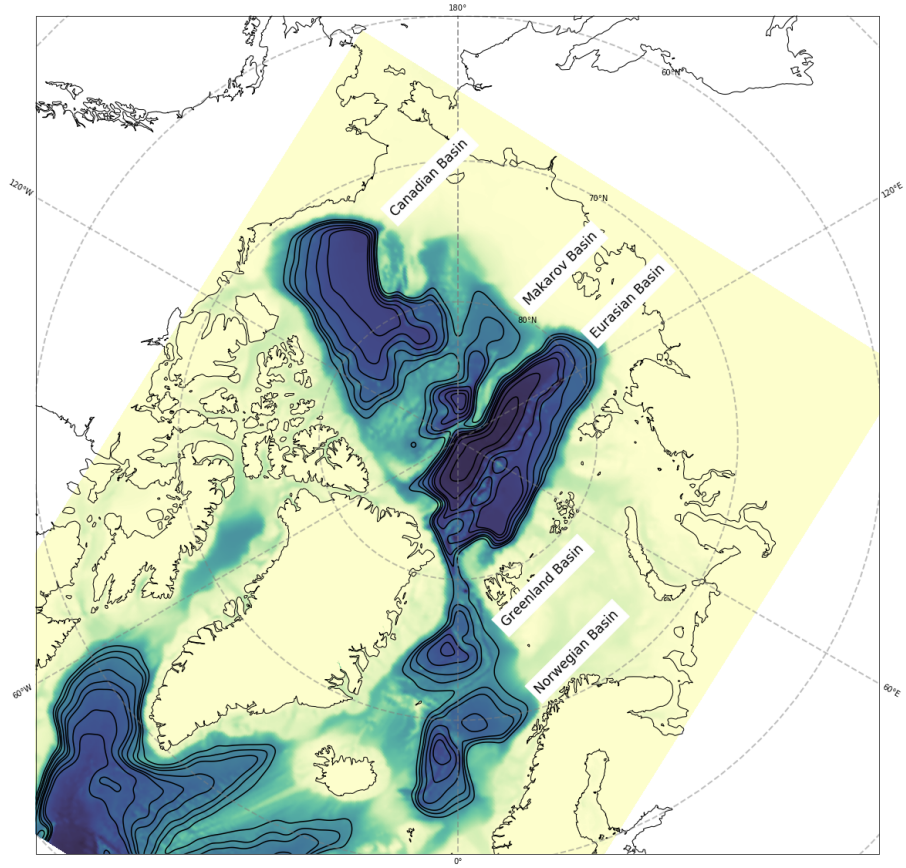

Figure 1.1: Overview of the study region. The five ocean basins, and the geostrophic contours studied, are shown. The open contours in the lower left of the figure are outside the field of study.

correspondence between the actual velocities in the ocean and calculations. In their study, a region was either fully covered by ice, or not at all. Regarding that the ocean may be partly covered, a sea-ice concentration-weighted surface stress could provide a more realistic response in ocean velocity. In mathematical terms this surface stress parameterisation is $\boldsymbol{\tau}_o = \alpha\boldsymbol{\tau}_{io} + (1-\alpha)\boldsymbol{\tau}_{ao}$, which was used by Meneghello et al. (2018). Here $\boldsymbol{\tau}$ is a surface stress vector, α is the sea-ice concentration, and the subscripts denote **o**cean, **i**ce and **a**tmosphere. In an ocean model, other factors such as ice thickness and roughness may be included in the stress parameterisation as well.
A second hypothesis is that the inclusion of lateral vorticity fluxes could improve results. Allowing for eddy viscosity drag from the sides turns the theory nonlinear, and its inclusion is described in section 2.1.
Finally, allowing for a stratified ocean could mend the results for the Arctic, as the ocean in this region is significantly stratified, compared to the Nordic Seas.

In this thesis, the two first hypotheses are investigated, utilising data from a high resolution ocean model. Note that the hypotheses are not tested in the statistical sense, but rather commented upon in light of the results presented.

The comparison of model data and theory in Isachsen et al., 2003 was performed with model data on a grid with length scales of $O(100)$ km and with monthly values. In such a model, the mesoscale is not resolved, and thus no eddy activity can occur, and must be parameterised. Additionally, the large time scale also acts to even out chaotic behaviour. In this thesis, the model data has a spatial and temporal resolutions of $O(1-10)$ km and one day, respectively, and eddy activity is therefore resolved. Eddies are central to the existence of lateral vorticity fluxes. The studied model also includes the full surface stress.

The weakness in this model-only approach is that one gets no actual real-world data to work with. Though, when only viewing a *model reality* one has access to all variables an fields, which is an advantage for understanding the output.

Using the surface forcing of the high-resolution model in the following experiment largely confirmed theory. However, some unforeseen behaviour in the dynamics was found as well.

1.3 Outline

The remainder of this thesis is organised in the following manner, chapter 2 describes the theory, data and methods used in the study. Results are presented in chapter 3, and then discussed in chapter 4. Lastly, conclusions are drawn upon the study in chapter 5.

CHAPTER 2

Theory, data and methods

2.1 Theory

The theoretical model is developed from the linear shallow-water momentum equation, given as:

$$\frac{\partial \boldsymbol{u}}{\partial t} + \hat{\mathbf{k}} \times f\boldsymbol{u} = -g\nabla\eta + \frac{\boldsymbol{\tau}}{\rho H} - \frac{R\boldsymbol{u}}{H}. \tag{2.1}$$

As described previously, f and H denote the Coriolis parameter and depth, respectively, and $\boldsymbol{\tau}$ is the total surface stress vector. Further, $\boldsymbol{u}$ is the horizontal oceanic velocity vector, which is constant in depth, g constitutes the gravitational acceleration and η is the sea surface height. Finally, ρ is the constant ocean water density and R is the linear bottom Ekman stress parameter. The curl of equation 2.1 is the vorticity equation:

$$\frac{\partial}{\partial t}\nabla \times \boldsymbol{u} + \nabla \cdot f\boldsymbol{u} = \nabla \times \frac{\boldsymbol{\tau}}{\rho H} - \nabla \times \frac{R\boldsymbol{u}}{H}. \tag{2.2}$$

Equation 2.2 integrated about a closed contour gives:

$$\frac{\partial}{\partial t}\iint_C (\nabla \times \boldsymbol{u})\cdot \mathrm{d}\boldsymbol{a} + \iint_C \nabla \cdot f\boldsymbol{u}\mathrm{d}a = \iint_C \left(\nabla \times \frac{\boldsymbol{\tau}}{\rho H}\right)\cdot \mathrm{d}\boldsymbol{a} - \iint_C \left(\nabla \times \frac{R\boldsymbol{u}}{H}\right)\cdot \mathrm{d}\boldsymbol{a}.$$

Here the subscript C denotes the contour. Through Green's and Gauss' theorems the above equation can be rewritten to

$$\frac{\partial}{\partial t}\oint_C \boldsymbol{u}\cdot \mathrm{d}\boldsymbol{l} + \oint_C f\boldsymbol{u}\cdot\hat{\mathbf{n}}\mathrm{d}l = \oint_C \frac{\boldsymbol{\tau}}{\rho H}\cdot \mathrm{d}\boldsymbol{l} - \oint_C \frac{R\boldsymbol{u}}{H}\cdot \mathrm{d}\boldsymbol{l}. \tag{2.3}$$

Here, $\hat{\mathbf{n}}$ is the normal unit vector to the contour. As stated in section 1.1, the study will consider the dynamics of closed f/H-contours. If the contour is drawn about a constant f/H value, the rigid lid approximation gives that the second term vanishes,

$$\oint_C f\boldsymbol{u}\cdot\hat{\mathbf{n}}\mathrm{d}l = \frac{f}{H}\oint_C H\boldsymbol{u}\cdot\hat{\mathbf{n}}\mathrm{d}l = 0.$$

Since the contour is closed, there can be no net in- or outflow of water in the volume it encompasses, if the sea-level is set. The integral balance 2.3 does

not demand that flow follows the contour in every point, but solves for the average along-contour flow. An important assumption is that this theory holds for large-scale circulation. To facilitate for this, the mesoscale variations in bathymetry must be smoothed for a realistic ocean. This process is described in section 2.2.

Isachsen et al. (2003) argued further for along f/H-contour motion. They nondimensionalised equation 2.2 and found a common damping parameter that was present in each term of the balance, except for the Coriolis term. Assuming weak damping, they could argue that the streamlines for a first order transport was along the f/H-contours. The transport stream function is defined as $H\boldsymbol{u}_0 = \hat{\mathbf{k}} \times \nabla\Psi$. Under their assumptions the transport stream function is a function of f/H, $\Psi = \Psi(f/H)$, where $H\boldsymbol{u}_0 = \hat{\mathbf{k}} \times \nabla\Psi = \Psi' \hat{\mathbf{k}} \times \nabla(f/H)$. The subscript 0 in the previous relations denotes the first order, and the prime is differentiation in Newton's notation. This result is very useful when comparing the calculation to observations from transects in ocean basins, as one assumes along-contour motion in each data point. However, in this study, only model data is compared. Therefore, the assumption of a first order flow parallel to the contours is not necessary to introduce.

This study differs further from Isachsen et al. (2003). By assuming temporal periodicity in all variables, and Fourier transforming them, they arrived at

$$\frac{\partial\Psi}{\partial q} = \Re\left[\frac{\oint \frac{\boldsymbol{\tau}}{\rho H} \cdot \mathrm{d}\boldsymbol{l}}{\oint \left(\frac{R}{H^2} + \frac{i\omega}{H}\right) \hat{\mathbf{k}} \times \nabla q \cdot \mathrm{d}\boldsymbol{l}}\right]. \tag{2.4}$$

The $\boldsymbol{\tau}$ in the above expression is the Fourier transformed surface stress, ω is the angular frequency in the first-order velocity and $q = f/H$. The equation describes the change of transport stream function along a gradient of f/H-values. Note that only the real part of the RHS in equation 2.4 contributes.

In this study a different method was favoured. By bringing the second term on the RHS to the LHS of equation 2.3, one obtains:

$$\oint_C \left[\frac{\partial \boldsymbol{u}}{\partial t} + \frac{R\boldsymbol{u}}{H}\right] \cdot \mathrm{d}\boldsymbol{l} = \oint_C \frac{\boldsymbol{\tau}}{\rho H} \cdot \mathrm{d}\boldsymbol{l}. \tag{2.5}$$

With integrating factor $\exp(Rt/H)$, and operating on the f-plane, direct integration in time yields

$$\oint_C \boldsymbol{u}(T) \cdot \mathrm{d}\boldsymbol{l} = e^{-\frac{RT}{H}} \oint_C \left[\int_0^T e^{\frac{Rt}{H}} \frac{\boldsymbol{\tau}}{\rho H} \mathrm{d}t + \boldsymbol{u}(0)\right] \cdot \mathrm{d}\boldsymbol{l}. \tag{2.6}$$

Where $\oint_C \boldsymbol{u}(0) \cdot \mathrm{d}\boldsymbol{l}$ is the initial condition. If weighted by $1/L$, with L as the contour length, this relation states that the along contour velocity at time T is proportional to the cumulative along contour surface stress, weighted by an exponential function of the bottom friction spin-down period H/R. No assumptions about the surface stress or velocity are made, and the only unknown parameter is the bottom friction R.

Lateral vorticity fluxes

The inclusion of lateral vorticity fluxes, due to eddy activity in the ocean, could prove to yield more realistic results for the circulation about a contour. By

adding the term $\hat{\mathbf{k}} \times \zeta \boldsymbol{u}$ on the LHS of equation 2.1, with $\zeta = \frac{\partial v}{\partial x} - \frac{\partial u}{\partial y}$ as the relative vorticity, one has the total vorticity in the shallow-water equation. With this addition, the relation 2.3 becomes

$$\frac{\partial}{\partial t} \oint_C \boldsymbol{u} \cdot \mathrm{d}\boldsymbol{l} + \oint_C \zeta \boldsymbol{u} \cdot \hat{\mathbf{n}} \mathrm{d}l = \oint_C \frac{\boldsymbol{\tau}}{\rho H} \cdot \mathrm{d}\boldsymbol{l} - \oint_C \frac{R\boldsymbol{u}}{H} \cdot \mathrm{d}\boldsymbol{l}. \tag{2.7}$$

The $\zeta \boldsymbol{u}$-term is nonlinear, as the ocean velocity is multiplied by itself. Therefore, there is no analytical way forward from this. The terms of equation 2.7 will be compared in the analysis, to assess their relative contributions.

2.2 Model data

The data used to test the theory comes from the Arctic4 run, produced by the Norwegian Polar Institute, of the Regional Ocean Modelling System (ROMS) Ocean Model. The model grid lies on a polar stereographic projection with a spatial resolution of about 4 km. As it is the large-scale circulation that is studied, the bathymetry was smoothed by a two-dimensional Gaussian filter with a kernel of ten points, equalling roughly 40 km. In addition, data arrays for the Coriolis parameter, f, and f/H, with the smoothed depth, were created. The next step was to decide on the constant f/H values to draw contours on. The contour set is made up of eight f/H-values that were chosen such that each ocean basin of interest has some closed contours and is bounded by at least one open contour. To simplify interpolation to f/H-contours, all data points were regridded to the same coordinates. Following this, the entire time-series was interpolated to the chosen contours. In sum, data was stripped down to only the necessary components to let the analysis be as efficient as possible. The available data are a time series of 1926 points, with one time step being the average of 24 hours. This equals roughly five years worth of data. Only the final 1044 time steps include the vorticity fields, which amounts to approximately three years.

2.3 Methods

To solve equation 2.6 with the available data, it was discretised to

$$\sum_C \boldsymbol{u}(T) \cdot \Delta \boldsymbol{l} = e^{-\frac{RT}{H}} \sum_C \left[\sum_{n=1}^{N} e^{\frac{Rt_n}{H}} \frac{\boldsymbol{\tau}_n}{\rho H} \Delta t + \boldsymbol{u}(0) \right] \cdot \Delta \boldsymbol{l}. \tag{2.8}$$

The N denotes the amount of time steps leading to time T. As the time-integral in equation 2.6 is zero at time 0, the time-sum here runs from the second time-step (n is zero-indexed). Switching the order of summation on the RHS of equation 2.8 facilitates for extracting circulation results for each time step while iterating through the time series,

$$\sum_C \boldsymbol{u}(T) \cdot \Delta \boldsymbol{l} = e^{-\frac{RT}{H}} \left[\sum_C \boldsymbol{u}(0) \Delta \boldsymbol{l} + \sum_{n=1}^{N} \sum_C e^{\frac{Rt_n}{H}} \frac{\boldsymbol{\tau}_n}{\rho H} \cdot \Delta \boldsymbol{l} \Delta t \right]. \tag{2.9}$$

The output of the equation above has the unit m^2/s, but it is desirable to get the output as an average velocity for the contour. Thus, both sides of

the equation were multiplied by $1/L$, with L as the contour length. The final balance is then

$$\frac{1}{L}\sum_C \boldsymbol{u}(T)\cdot\Delta\boldsymbol{l} = \frac{e^{-\frac{RT}{H}}}{L}\left[\sum_C \boldsymbol{u}(0)\Delta\boldsymbol{l} + \sum_{n=1}^{N}\sum_C e^{\frac{Rt_n}{H}}\frac{\boldsymbol{\tau}_n}{\rho H}\cdot\Delta\boldsymbol{l}\Delta t\right] \tag{2.10}$$

The LHS of equation 2.10 was fed with the actual velocity data from the model time series, in the numerical routines, to use as comparison for the RHS solutions. On the RHS, the term including $\boldsymbol{u}(0)$ effectively sets the linear solution to the model state for the first time-step.

To examine the relative contribution of the terms of equation 2.7, it was discretised to

$$\sum_C \frac{\boldsymbol{u}_t - \boldsymbol{u}_{t-1}}{\Delta t}\cdot\Delta\boldsymbol{l} + \sum_C \zeta_t\boldsymbol{u}_t\cdot\hat{\mathbf{n}}\Delta l = \sum_C \frac{\boldsymbol{\tau}_t}{\rho H}\cdot\Delta\boldsymbol{l} - \sum_C \frac{R\boldsymbol{u}_t}{H}\cdot\Delta\boldsymbol{l}. \tag{2.11}$$

In the above expression, the subscript t denotes the time step of interest. When iterating through the time series, the time derivative in the first term demands knowledge about the previous time step. All other terms only take in the instantaneous data.
For the whole analysis, the ocean density was set at $\rho = 1027.5$ kg/m^3.

Analytical example

To test the numerical routines for solving equation 2.10, two simplified data sets were created. The data points lie on a square grid of 99 by 99 points with a 3 km inter-point distance, where the centre of the grid represents the North Pole. These data sets share a circular bathymetry about the North Pole and both have a circular wind stress atop. The two wind stress sets and bathymetry are given as

$$\boldsymbol{\tau}(r) = Ar\hat{\mathbf{t}}, \text{ and } \boldsymbol{\tau}(r,t) = Ar\sin\omega t\hat{\mathbf{t}}$$
$$H(r) = H_0 e^{-\frac{r^2}{r_{max}^2}}.$$

Here $A = \tau_{max}/r_{max}$ is a scaling factor for the cyclone, r is the distance from the vortex centre, H_0 is the maximal depth, and t is the time since initialisation. The maximal surface stress is set at $\tau_{max} = 0.1$ Pa, and maximal radius is given by the grid, i.e. $r_{max} = \sqrt{2}\times 49\times 3$ km. The bathymetry resembles a circular Gaussian bell, with its deepest point in the centre, at the model North Pole. The surface forcing, $\boldsymbol{\tau}$, only has a component in the azimuthal direction and is cyclonic for positive values This is specified with the tangential unit vector $\hat{\mathbf{t}}$. The two stress examples represent a step-function and a sinusoidal variation in surface stress, respectively. At $t = 0$ the ocean is at rest. With these surface stress and bathymetry parameters as input to equation 2.6, it can be solved analytically as

$$\boldsymbol{u} = \frac{Ar}{\rho R}\left[1 - e^{-\frac{Rt}{H}}\right], \tag{2.12}$$

for the step function surface stress, and

$$\boldsymbol{u} = \frac{Ar}{\rho H}\frac{1}{\left(\frac{R}{H}\right)^2 + \omega^2}\left[\frac{R}{H}\sin\omega t - \omega\cos\omega t + \omega e^{-\frac{Rt}{H}}\right], \tag{2.13}$$

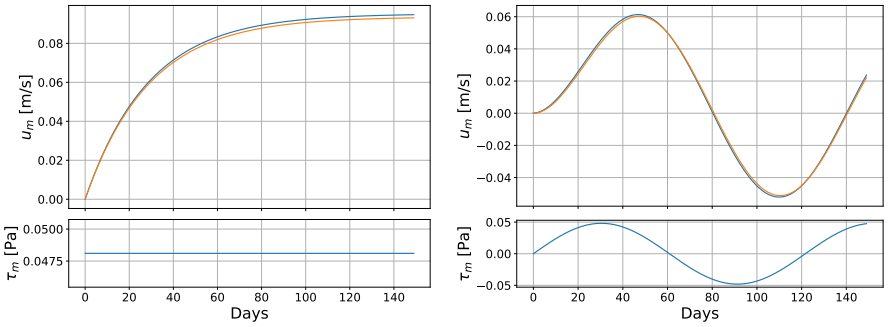

(a) (b)

Figure 2.1: Circulation plots for the idealised analytical cases. In the top plots the blue line represents the solution of equation 2.10, while the orange line in (a) holds the result to 2.12, and in (b) to equation 2.13. The lower subplots display the surface stress acted upon the fluid.

for the sinusoidal wind forcing.

Setting $H_0 = 5000$ m, $R = 5 \times 10^{-4}$ m/s, ω at six cycles per year and $r = 100$ km, equations 2.12 and 2.13 were solved for the 150 time steps, with one time step representing 24 hours. Equation 2.10 was solved for the same parameters. The theoretical and numerical results are presented in figure 2.1.

Both figures 2.1a and 2.1b show that the script captures the theoretical response to the surface stress, and thus validate the functionality.

Viewing figure 2.1b, the first peak for the surface stress is at about day 30, while the first peak in circulation happens at day 45. The spin up period is $H/R \approx 28$ days, and acts to delay the response in the ocean.

CHAPTER 3

Results

Due to a mistake in the deduction of equation 2.6, the results presented in this section are solutions to

$$\frac{e^{\frac{-RT}{H}}}{L}\sum_C e^{\frac{RT}{H}}\boldsymbol{u}\cdot\Delta\boldsymbol{l} = \frac{e^{\frac{-RT}{H}}}{L}\left[\sum_C \boldsymbol{u}(0)\Delta\boldsymbol{l} + \sum_{n=1}^{N}\sum_C e^{\frac{Rt_n}{H}}\frac{\boldsymbol{\tau}_n}{\rho H}\cdot\Delta\boldsymbol{l}\Delta t\right], \quad (3.1)$$

which is a wrongful expression of equation 2.10. The mistake was not working on the f-plane and allowing the integrating factor $exp(Rt/H)$ to pass through the integral on the RHS. This is not mathematically sound. The factor multiplied to each side of equation 3.1 is there to get the output as an average along-contour velocity. Although the expression above is not mathematically correct, the differences between this and equation 2.10 should not be crucial to the analysis, at least qualitatively. The mistake was discovered at a stage in the work where it was virtually impossible to remake the results.

Equation 3.1 was solved for f/H-contours in five major ocean basins in the Nordic Seas and Arctic Ocean, presented in figure 1.1. To find the best bottom friction parameter, R, for each contour, an array of different values for R was created. All contours were checked for all R-values, and the result with the best correlation between the LHS and RHS of equation 3.1 was picked. As of this point, the left hand side of equation 3.1 will be referred to as *ROMS velocity data* and similar terms, and the right hand side will be named the *linear model*.

Table 3.1 holds information for each f/H-contour studied. The range in depth goes from about 4000 metres for the deepest contour of the Eurasian Basin, to about 2000 metres for the contour surrounding the study area.

The comparisons between ROMS ocean velocities and the linear model results will be presented in three frameworks. First, the time series of the linear model results and the ROMS model velocity data for all contours are presented in section 3.1. Then, coherence magnitudes for each basin are provided in section 3.2, to investigate how the linear model compares to the ROMS data in terms of temporal variability. Thirdly, scatter plots of the time series are presented in section 3.3, to shed light on which values of the linear model have the best correspondence with the ROMS data. Finally, the vorticity flux intrusion, described in 2.1, is presented for the Norwegian and Canadian Basins in section 3.4. In the following sections, all references to positive motion, means that it is cyclonic, and vice versa for negative motion.

Contour nr.	**Basin**	f/H**-value** [ms^{-1}]	**Information**
0	Eurasian Basin	3.43×10^{-8}	Amundsen Basin
1	Eurasian Basin	3.6×10^{-8}	Amundsen Basin
2	Norwegian Basin	3.85×10^{-8}	-
3	Eurasian Basin	3.85×10^{-8}	Nansen Basin
4	Eurasian Basin	3.85×10^{-8}	Amundsen Basin
5	Makarov Basin	3.85×10^{-8}	-
6	Canadian Basin	3.85×10^{-8}	-
7	Norwegian Basin	4.0×10^{-8}	-
8	Greenland Basin	4.0×10^{-8}	-
9	Eurasian Basin	4.0×10^{-8}	-
10	Eurasian Basin	4.0×10^{-8}	About mount
11	Eurasian Basin	4.0×10^{-8}	About mount
12	Makarov Basin	4.0×10^{-8}	-
13	Canadian Basin	4.0×10^{-8}	-
14	Norwegian Basin	4.3×10^{-8}	-
15	Norwegian Basin	4.3×10^{-8}	Lofoten Basin
16	Greenland Basin	4.3×10^{-8}	-
17	Eurasian Basin	4.3×10^{-8}	-
18	Makarov Basin	4.3×10^{-8}	-
19	Canadian Basin	4.3×10^{-8}	-
20	Norwegian Basin	4.8×10^{-8}	-
21	Greenland Basin	4.8×10^{-8}	-
22	Eurasian Basin	4.8×10^{-8}	-
23	Makarov Basin	4.8×10^{-8}	-
24	Canadian Basin	4.8×10^{-8}	-
25	Norwegian Basin	5.2×10^{-8}	-
26	Greenland Basin	5.2×10^{-8}	-
27	Eurasian Basin	5.2×10^{-8}	Also MB
28	Canadian Basin	5.2×10^{-8}	-
29	Whole Region	6.0×10^{-8}	-

Table 3.1: Overview of the f/H-contours investigated in the project. The Amundsen and Nansen Basins are deep basins within the Eurasian Basin, and the Lofoten Basin is a sub-basin in the North-East of the Norwegian Basin (see figure 1.1). Contour 27 is drawn within both the Eurasian and Makarov Basins. Where *About mount* has been noted, the contour is drawn about a seamount rather than a basin, and the study will not consider these contours.

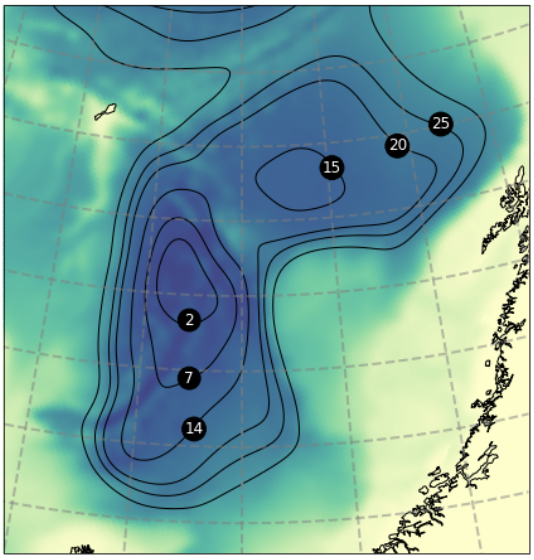

Figure 3.1: Map of the Norwegian Basin. The f/H contours of the basin are numbered in the fashion presented in table 3.1. Contour 15 lies entirely within the Lofoten Basin.

3.1 Time series and correlations

Nordic Seas basins

The time-series with the optimal R-value, for the contours of the Norwegian and Greenland Basins are presented in this section. Starting with the Norwegian Basin contours (figure 3.1), the linear model responds to the surface stress as expected, when viewing equation 3.1. For periods of strong surface forcing the circulation intensifies, and when forcing is weak the bottom stress decelerates the flow. Compared to the ROMS model data, the variability seems to be quite well captured. For all contours, the average circulation is cyclonic, with anticyclonic motion confined only to brief periods. The linear model seems to overestimate both the amount of and intensity of anticyclonic episodes. Temporal averages of the surface stress are positive (cyclonic) for all contours in the Norwegian Basin. For the three deepest contours (3.2a, 3.2b and 3.2c) the linear model results consistently lies below or above the ROMS model data, for the highest correlation R-value. For the more shallow contours (3.2e and 3.2f), the linear model tends to amplify both the peaks and troughs. The circulation results for contour in the Lofoten Basin (3.2d) follow each other quite closely, for the same value of R as the corresponding Norwegian Basin contour. The highest correlation values of R are presented in table 3.2, along with the correlation itself. The average correlation for the Norwegian Basin is 0.893.

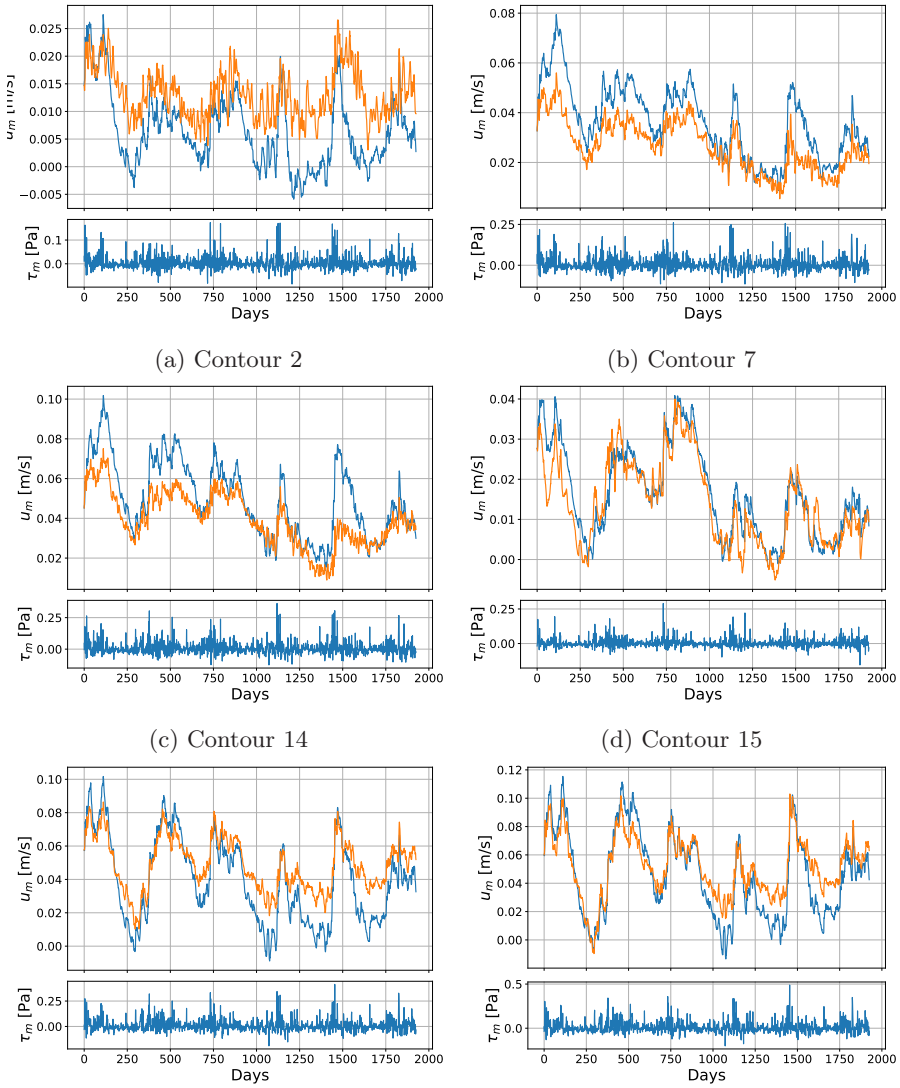

(a) Contour 2

(b) Contour 7

(c) Contour 14

(d) Contour 15

(e) Contour 20

(f) Contour 25

Figure 3.2: Circulation data for the contours in the Norwegian Basin. For each plot the the blue and orange lines in the top plot represent the linear model and ROMS model velocity data, respectively. The lower plots display the average wind stress about the corresponding contour. Sub-figure 3.2d presents results for the Lofoten basin.

Contour	R**-value** [m/s]	**Correlation**
2	5×10^{-4}	0.728
7	1.5×10^{-4}	0.938
14	1.5×10^{-4}	0.882
15	1.5×10^{-4}	0.916
20	2.5×10^{-4}	0.955
25	2.5×10^{-4}	0.938

Table 3.2: Overview of the R-values that yield the highest correlations between the LHS and RHS of equation 2.10, for contours in the Norwegian Basin.

Contour	R**-value** [m/s]	**Correlation**
8	1×10^{-4}	0.846
16	2.5×10^{-4}	0.881
21	5×10^{-4}	0.926
26	2.5×10^{-4}	0.959

Table 3.3: Overview of the R-values that yield the highest correlations between the LHS and RHS of equation 2.10, for contours in the Greenland Basin.

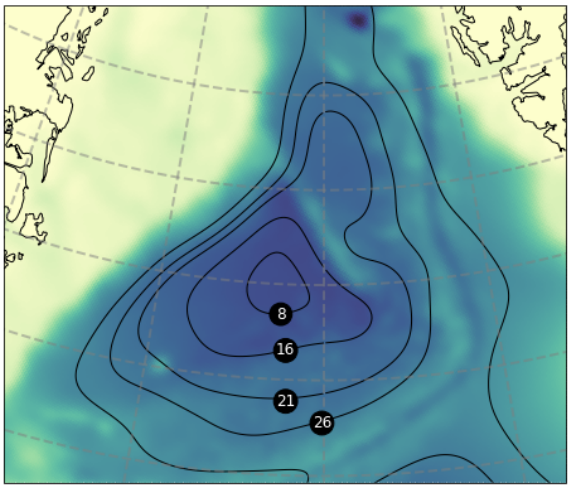

Figure 3.3: Map of the Greenland Basin. The contours in the basin are numbered as in table 3.1.

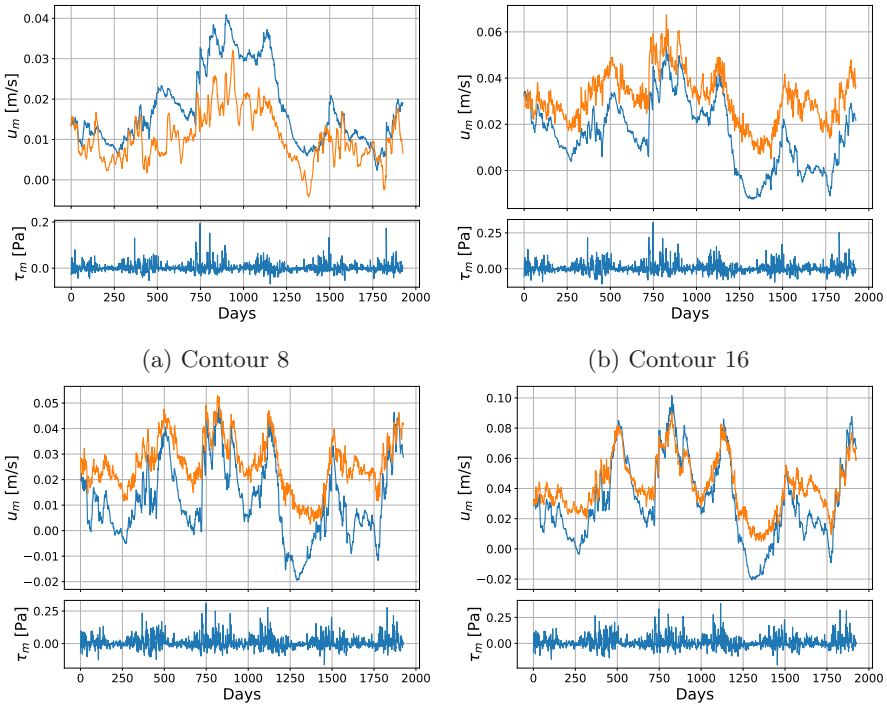

(a) Contour 8

(b) Contour 16

(c) Contour 21

(d) Contour 26

Figure 3.4: Circulation data for the contours in the Greenland Basin. The layout is the same as in figure 3.2.

Figure 3.3 displays an overview of the Greenland Basin, including the contours investigated. The results for the Greenland Basin (figure 3.4) resemble those for the Norwegian Basin, and the same general remarks can be made for both. For the deepest contour (3.4a), R is set at a comparably low value of 1×10^{-4} m/s, and the linear model data is as such positively exaggerated compared to the ROMS data. For the remaining contours, R is larger, and the linear model has more reserved amplitudes for the peaks. The local minima for circulation are again exaggerated by the linear model, but peaks seem to correspond quite well, particularly in contour 26 (3.4d). This contour has the overall highest correlation in this study, with a value of 0.959. The average correlation for the Greenland Basin is 0.903 (see table 3.3 for ideal R-values and correlations for the Greenland Basin). As for the Norwegian Basin, the time-averaged surface stress is positive for all contours.

Arctic Ocean basins

Results for the three basins of the Arctic Ocean are displayed in this section. An overview of the contours in the Eurasian and Makarov Basins is given in figure 3.5. Results for the Eurasian Basin are provided in figure 3.6.

The linear model, when it predicts cyclonic results, seems to capture the ROMS data's circulation. However, when the linear model transitions to anticyclonic

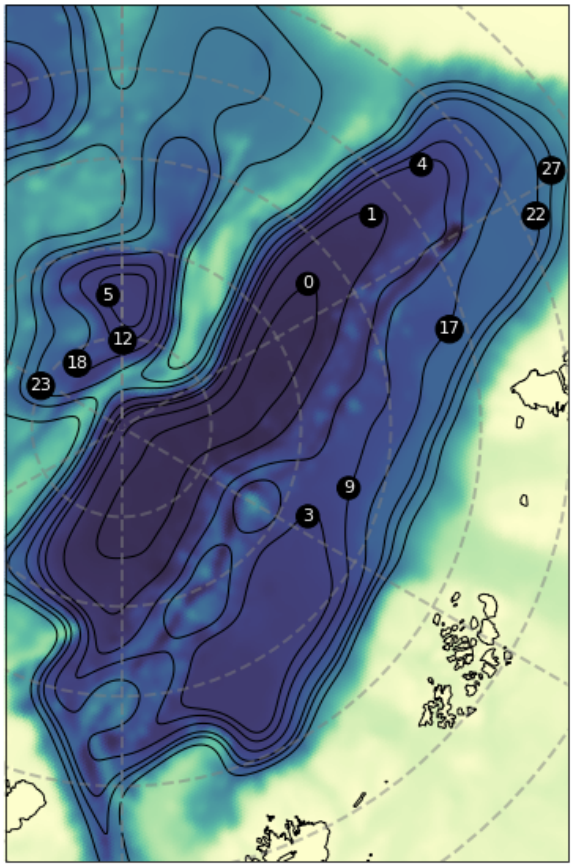

Figure 3.5: Map of the Eurasian and Makarov Basins. Contour numbers correspond to those in table 3.1. Note that contours 0 and 1 lie within the Amundsen Basin, and contour 3 lies within the Nansen Basin.

motion, the results do not match - oftentimes the two models have different signs when this is the case. For some contours, e.g. 3.6c and 3.6e, the linear model manages to catch up to the ROMS data after an anticyclonic period. The response to the surface stress in the linear model is more dramatic, with larger amplitudes, than for the ROMS data. Despite the discrepancies, correlations are above 0.79 for all but one contour in the basin with an average value of 0.825. Table 3.4 contains all correlation data for the Eurasian Basin. Only the two deep contours in the Amundsen Basin have a mean cyclonic surface stress, though the mean circulation in the ROMS data is cyclonic for all contours.

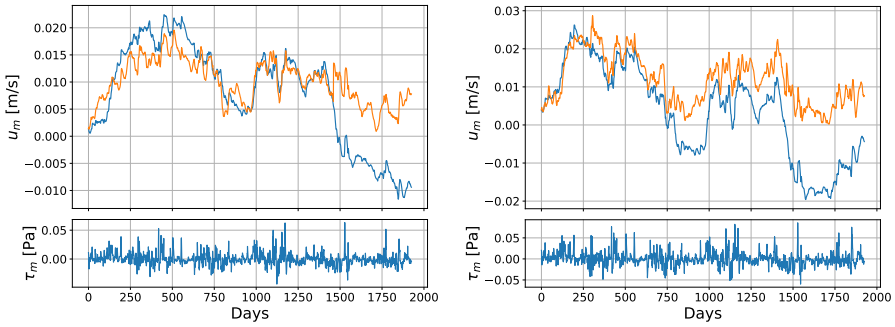

(a) Contour 0

(b) Contour 1

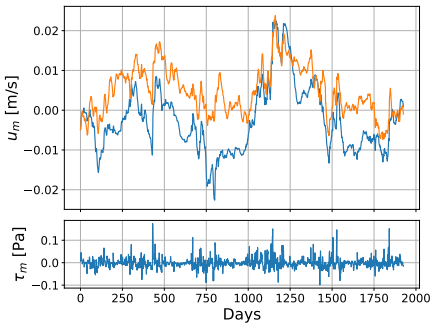

(c) Contour 3

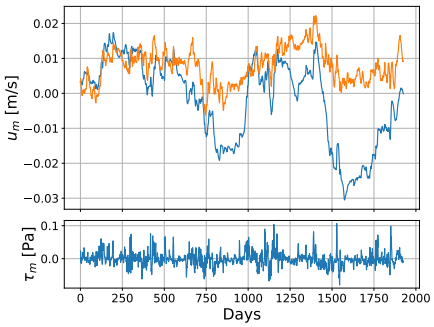

(d) Contour 4

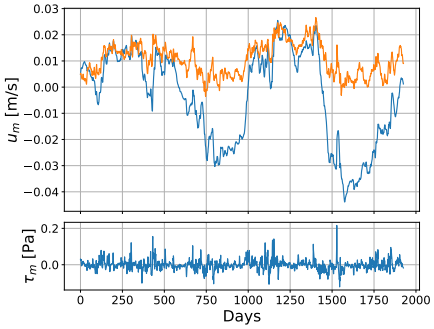

(e) Contour 9

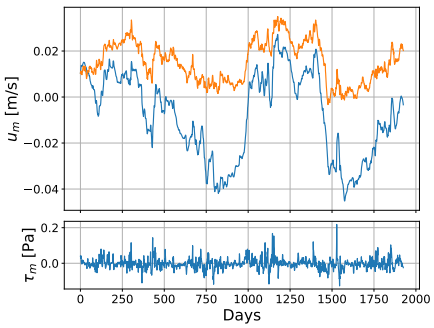

(f) Contour 17

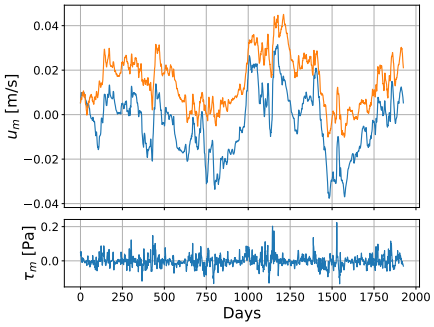

(g) Contour 22

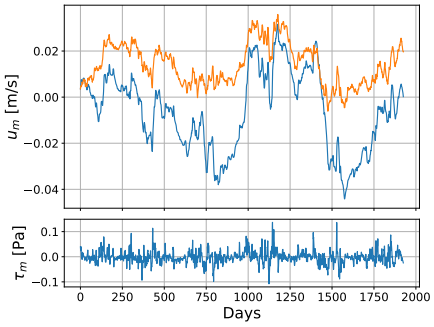

(h) Contour 27

Figure 3.6: Eurasian Basin circulation data. The layout follows that of figure 3.2.

Contour	R**-value** [m/s]	**Correlation**
0	0.5×10^{-4}	0.840
1	2×10^{-4}	0.873
3	2.5×10^{-4}	0.793
4	2.5×10^{-4}	0.595
9	2.5×10^{-4}	0.834
17	2.5×10^{-4}	0.912
22	5×10^{-4}	0.894
27	2.5×10^{-4}	0.860

Table 3.4: Overview of the R-values that yield the highest correlations between the LHS and RHS of equation 2.10, for contours in the Eurasian Basin.

Contour	R**-value** [m/s]	**Correlation**
5	15×10^{-4}	0.079
12	0.5×10^{-4}	0.227
18	0.5×10^{-4}	0.481
23	0.5×10^{-4}	0.751

Table 3.5: Overview of the R-values that yield the highest correlations between the LHS and RHS of equation 2.10, for contours in the Makarov Basin.

Contour	R**-value** [m/s]	**Correlation**
6	2.5×10^{-4}	0.448
13	10×10^{-4}	0.457
19	5×10^{-4}	0.825
24	5×10^{-4}	0.837
28	2.5×10^{-4}	0.832

Table 3.6: Overview of the R-values that yield the highest correlations between the LHS and RHS of equation 2.10, for contours in the Canadian Basin.

The Makarov Basin has quite ambiguous results, shown in figure 3.7, and the correlations for the four contours of the basin are given in table 3.5. Contour 5 (3.7a) has a "best" correlation for $R = 15 \times 10^{-4}$ m/s, thirty times higher than the best R-value for the remaining contours. It is obvious that the linear model is dampened to unrealistically low velocities, and this result cannot be viewed as representative (particularly since the correlation is only 0.08). When testing for values of R, some yielded negative correlation between the two models' data. Only circulation about the largest contour, 3.7d, has correlation above 0.7, and shows some of the same behaviour as was observed in the Eurasian Basin. Here, the linear model deviates to negative (anticyclonic) motion, while the ROMS data stays positive, but when it turns cyclonic the results correspond quite well. On average, the surface stress for all but contour 12, (3.7b) is anticyclonic.

Figure 3.8 displays the studied contours within the Canadian Basin. The circulation results for this basin have the most anticyclonic flow of the studied basins, as seen in figure 3.9. For the deepest contours, cyclonic and anticyclonic circulation are approximately evenly distributed in the ROMS data time series. With shallower water, the share of anticyclonic motion increases, where it for

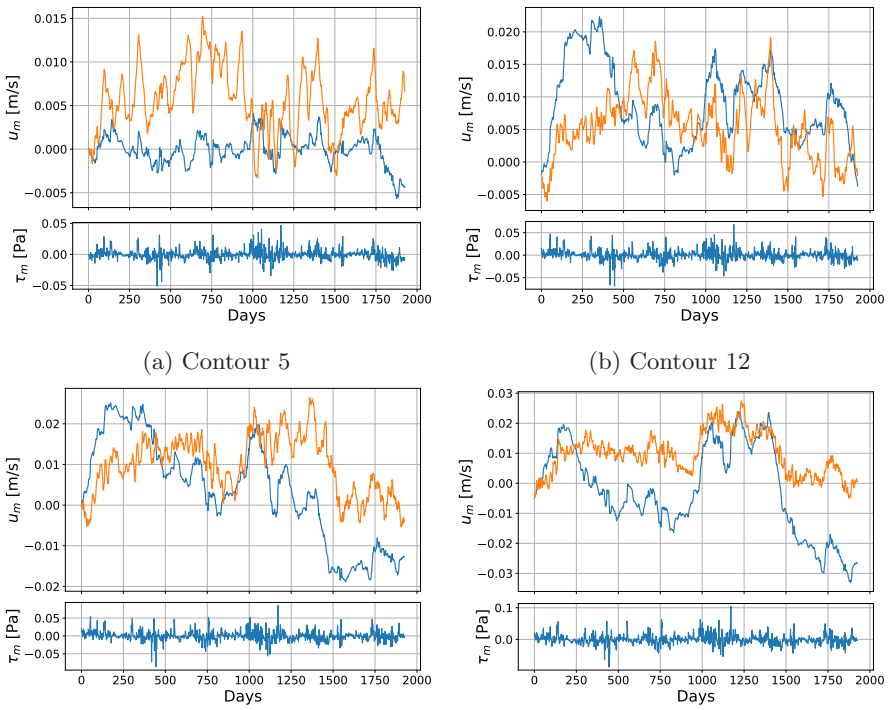

(a) Contour 5

(b) Contour 12

(c) Contour 18

(d) Contour 23

Figure 3.7: Makarov Basin circulation data. The layout follows that of figure 3.2.

contour 28 dominates the time series (figure 3.9e). The linear model overstates the negativity of the flow, compared to the ROMS data, responding heavily to strong negative forcing. In terms of correlation, the results improve with contour size, with values above 0.8 for the three shallowest contours. However, the time series for the two deepest contours have correlation at around 0.45, see table 3.6. The time-averaged surface stress is anticyclonic for the whole basin.

3.2 Coherence plots

Figure 3.10 shows the coherence magnitude plots for each basin. The coherence for each contour was calculated and then averaged by basin for each frequency. It is evident that the calculation performs well, coherence wise, for the Norwegian (3.10a), Greenland (3.10b) and Eurasian Basins (3.10d) above time scales of about 5-10 days. The result for the Canadian Basin (3.10c) is not as high as for the other three. For the Makarov Basin (3.10e), the coherence magnitudes reflect the poor results seen in the previous section, as the variability seems not to be captured at any time scales. Especially the Norwegian basin has a high coherence, with values between $0.5 - 0.9$ in time scales between approximately 10 and 250 days. A peak in coherence, of 0.8 emerges at approximately 5 days, then a dip in skill, down to 0.5 at around 20 days. From this point, the skill improves for variations on time scales up to 250 days with a coherence

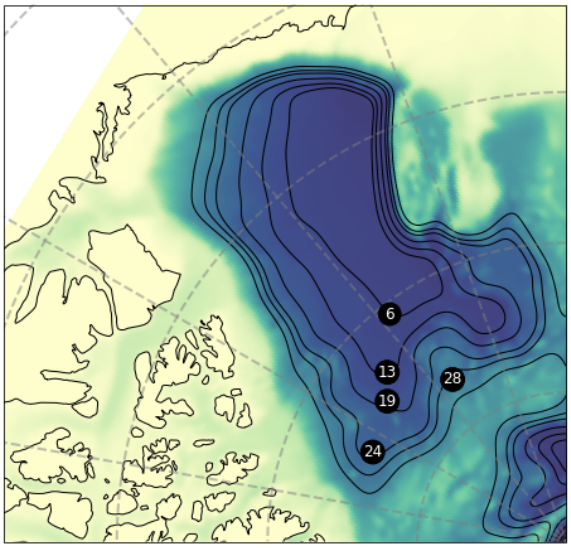

Figure 3.8: Map over the Canadian Basin. The contour numbers provided correspond to those in table 3.1.

approaching 0.9. The Greenland Basin follows the pattern of the Norwegian Basin, though with a peak at coherence 0.8 centered around 4 days. Then coherence drops off to about 0.4 for 10 days. Two peaks appear for time scales of 25 days and around a month, both at about 0.8. The trend for longer time scales approaches coherence values of 0.8. The Canadian Basin has quite chaotic results for time scales up towards 10 days, with generally low coherence values. A peak of 0.6 is present for temporal scales of 25 days. Coherence then drops towards 0.5 for time scales up towards 250 days. For the Eurasian Basin the coherence seems to gradually increase to around 0.6 for time scales up to about 10 days. From this point, the coherence oscillates about that value for all larger time scales. As mentioned, the coherence in the Makarov Basin is poor for most frequencies, which fits well with the results in figure 3.7.

3.3 Scatter plots

To examine the performance of the calculation for different along-contour velocities, scatter plots of the time series for the linear model and ROMS circulation results were made. Dividing these sets into the points where the linear model results are positive and negative, and performing a linear regression for each sign, can indicate in which of the modes the skill is highest or lowest. A slope close to 1:1, with interception near zero, and a slim spread in scattered points would indicate that the models match well.

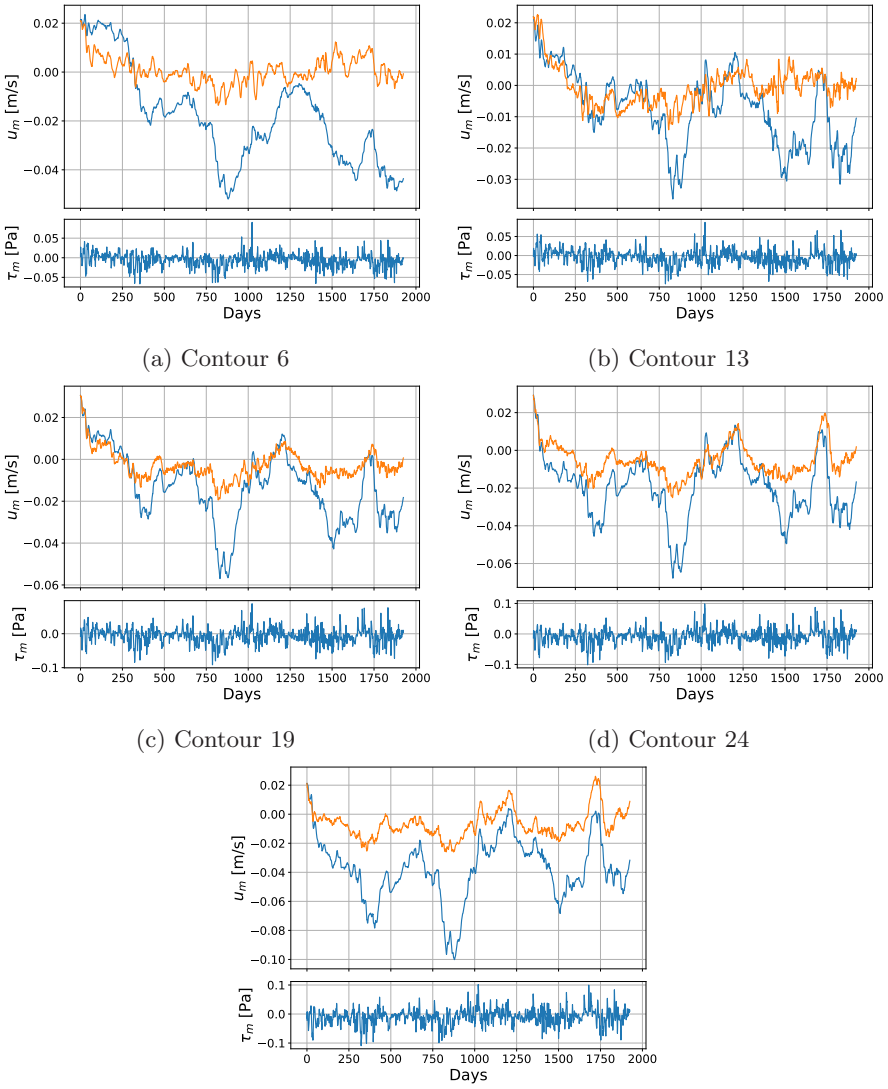

(a) Contour 6

(b) Contour 13

(c) Contour 19

(d) Contour 24

(e) Contour 28

Figure 3.9: Circulation data for the Canadian Basin. The layout follows that of figure 3.2.

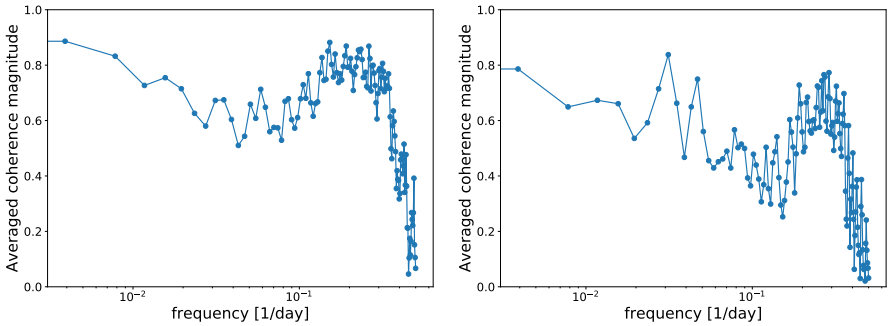

(a) Norwegian Basin

(b) Greenland Basin

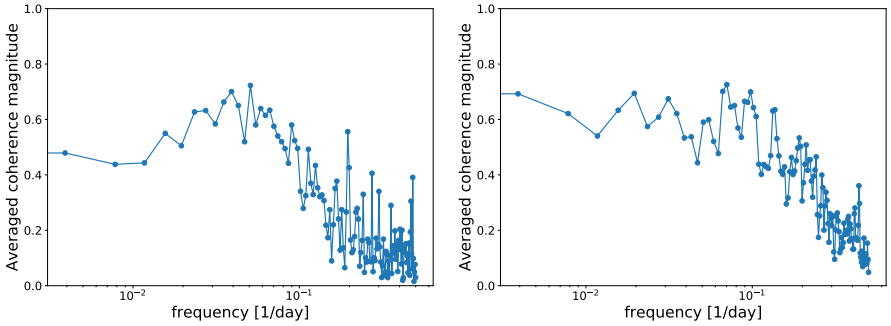

(c) Canadian Basin

(d) Eurasian Basin

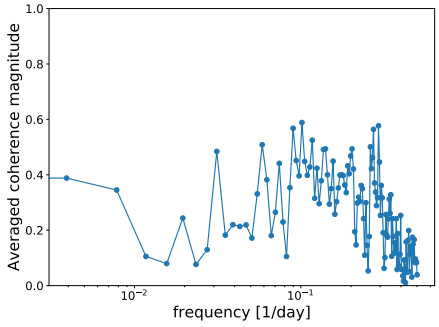

(e) Makarov Basin

Figure 3.10: Coherence magnitudes averaged for all contours in the given basin. The plot in (a) displays the values for the Norwegian Basin, (b) for the Greenland Basin, (c) for the Canadian Basin, (d) for the Eurasian Basin and finally (e) for the Makarov Basin.

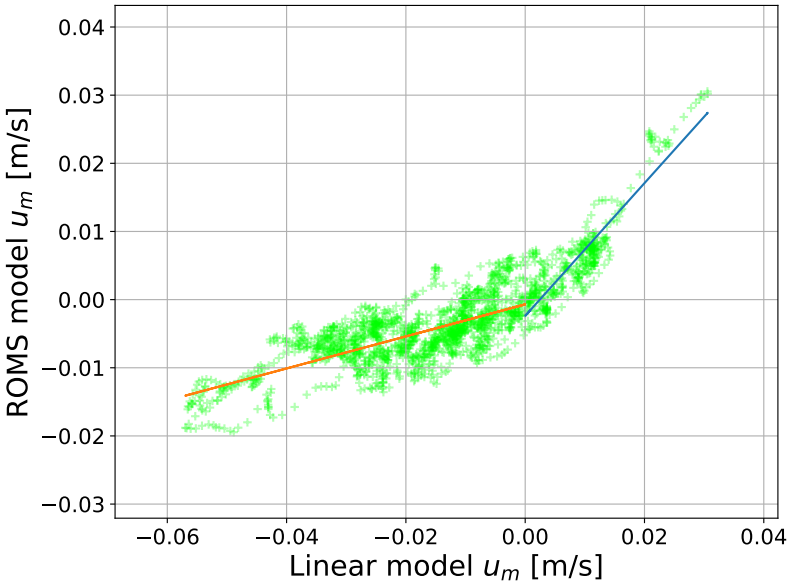

Figure 3.11: Scatter plot for contour 19, in the Canadian Basin. The calculated circulation lies on the horizontal axis, and the model circulation is on the vertical axis. Linear regression graphs for the values for when calculated circulation is positive and negative are displayed in blue and orange, respectively.

Figure 3.11 displays the scatter plot for contour 19, in the Canadian Basin. For the time steps when the linear model values are positive, the regression slope is 0.97, and when they are negative the slope is 0.23. Both graphs intercept quite close to zero. This result shows that when the linear model is anticyclonic, it greatly exaggerates the velocities compared to the model. However, when the calculation is positive, the two circulation results lie closer, on average.

The general tendency for anticyclonic circulation in the linear model is that it is too strong compared to the ROMS data. For the cyclonic case, the tendency is that low positive velocities are underestimated, and the peak velocities are exaggerated, as exemplified in figure 3.12 for contour 25, of the Norwegian Basin. Here, the slope for positive stress circulation values is 0.65, and one can see that the lowest positive values for the linear model circulation have larger corresponding ROMS model circulation values, and vice versa. Essentially, for positive circulation, the calculation amplifies both the highs and the lows. As seen for the circulation plots in section 3.1, the linear model often has to catch up to the ROMS data after an anticyclonic period only present for the linear data (see e.g. figure 3.6e for contour 9, of the Eurasian Basin around day 1000). This further flattens the curve for the positive results, as the linear model will always lie below the ROMS model in these catch-up phases. For negative circulation, the linear model almost always is too negative - often when the ROMS results are positive. These results correspond well to what was seen in section 3.1. Though here, it is clearer that the linear model indeed performs better for cyclonic flow, than for anticyclonic flow.

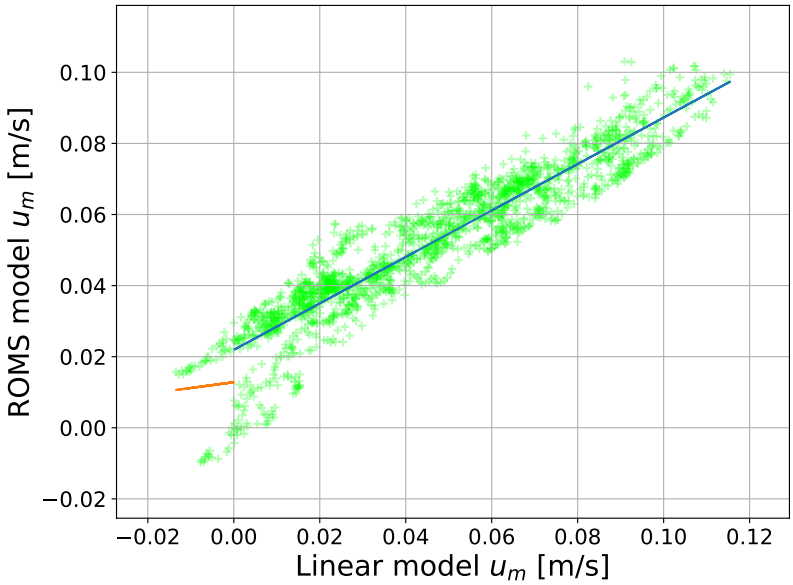

Figure 3.12: Scatter plot for contour 25, in the Norwegian Basin. This figure is organised in the same manner as figure 3.11.

3.4 Lateral vorticity fluxes

Returning to equation 2.11, the contribution from each of the terms were compared. If the equation captures all the dynamic drivers of the ROMS model, the sum of the terms should equate to zero. Figure 3.13 displays the solution to equation 2.11 in the deepest contour, number 2, of the Norwegian Basin for each time step where the vorticity fields were included (see section 2.2). All time series were smoothed with a ten point Gaussian filter, to even out some of the short term noise. The vorticity flux term completely dominates the relation, and thus the residual term compensates in a similar fashion. As seen in figure 3.2a the along-contour velocities are low compared to other, shallower, contours' velocities. The bottom stress parameter is positive at all times, reflecting that the flow is cyclonic throughout the time series. Components for the surface stress and time derivative are relatively small in this context, but they seem to work oppositely, which is expected.

For a larger and shallower contour (number 25) in the Norwegian Basin, the relative contribution from vorticity fluxes is diminished, as shown in figure 3.14. The magnitude of vorticity fluxes is comparable to that in contour 2, but on this contour the time derivative and surface stress terms, in particular, dominate. As those two terms act to cancel each other, the residual does not reach an amplitude comparable to the dominant terms. The bottom stress contribution clearly follows the sign of the time derivative term. This is visible, for instance, when the time derivative has its largest maximum.

Figure 3.15 displays the contribution of each term in 2.11 for the largest contour of the Canadian Basin, which is characterised by anticyclonic motion. The

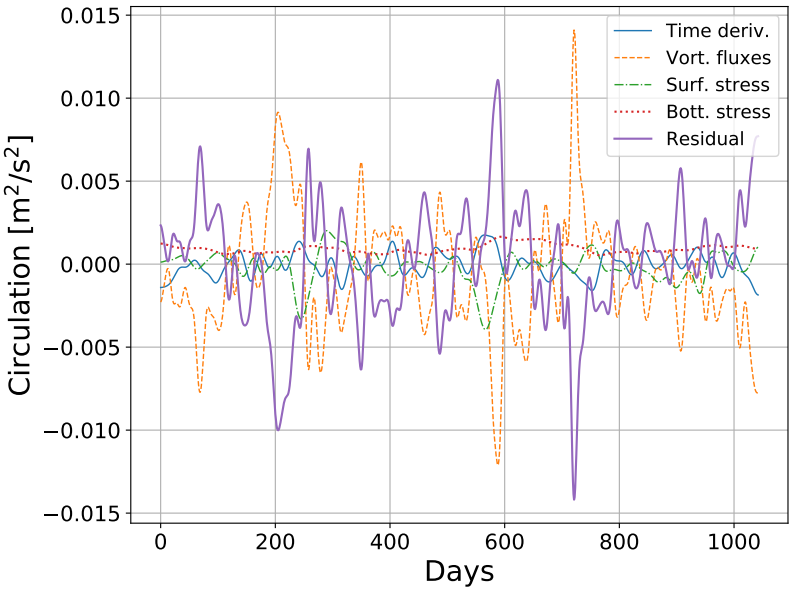

Figure 3.13: The time series for each term in equation 2.11, smoothed with a ten point Gaussian filter. The plot is for contour 2, in the Norwegian basin. All contributions were added together, and the residual is given as well.

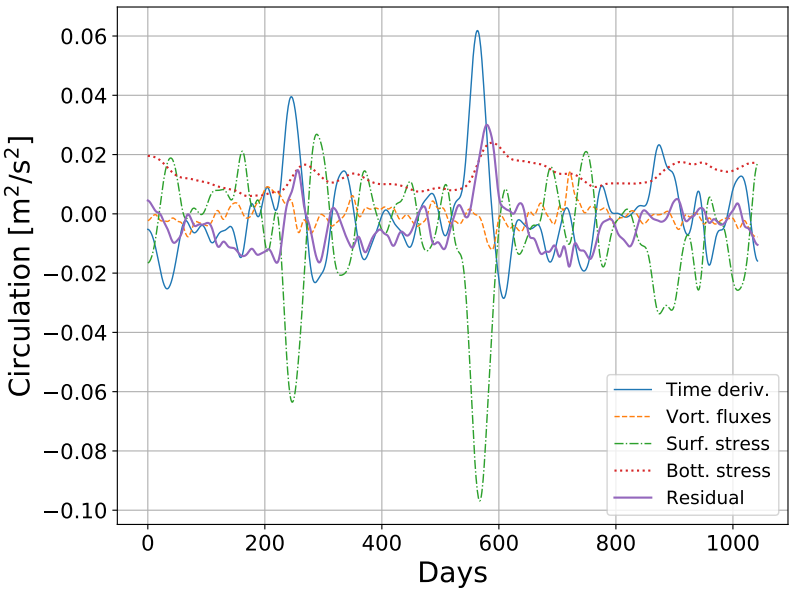

Figure 3.14: Similar to figure 3.13, here for the shallowest contour of the Norwegian Basin, number 25.

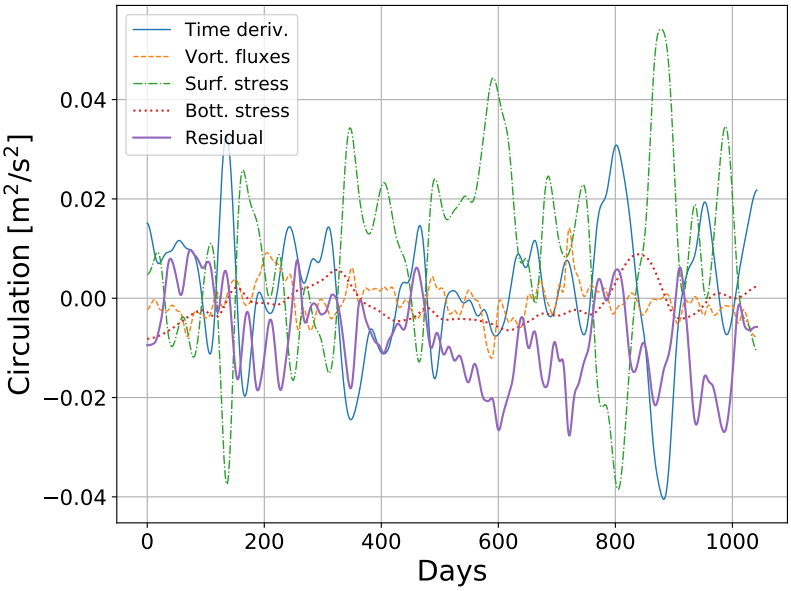

Figure 3.15: The integral balance for contour 28, in the Canadian Basin. Similar layout as figure 3.13.

frequent change of sign in the bottom friction contribution reflects that the circulation switches direction several times. Also here, the contribution from vorticity fluxes is small compared to those of both the time derivative and surface stress terms. The residual graph demonstrates that the integral balance does not encapsulate the full dynamics, as it is of comparable scale to the dominant terms. Thus, some other mechanism(s) is what impedes the circulation from responding linearly to anticyclonic surface stress.

CHAPTER 4

Discussion

While reading this section, keep in mind that any reference to the *linear model* is to equation 3.1, which is not mathematically correct. Though, the differences in output between that and equation 2.10 are minimal, due to the very weak variations in ocean depth along a contour.

4.1 Resolving hypotheses

As no rigorous statistical analyses have been performed to test the hypotheses, this section rather contains careful suggestions. The hypotheses for this study are given in section 1.2. In short, the first question is whether a more realistic surface stress parameterisation yields better results, particularly in the Eurasian Basin, than those found by Isachsen et al. (2003). The second question was whether the inclusion of lateral vorticity fluxes in the shallow-water equation improves the results overall for the basins studied. A final question of the effect of stratification was not explored in this study, but is touched upon later in the discussion.

In terms of correlation coefficients, the result for the first hypothesis is that the results were improved for the Eurasian Basin. The average correlation for this basin is 0.825, which is comparable to the results Isachsen et al. (2003) obtained for the Nordic Seas and considered successful. Coherence was consistently higher for the basin in this study as well, though within a different temporal spectrum than they obtained.

The inclusion of vorticity fluxes seems to not contribute much to the end solutions for circulation in the studied basins. However, it was discovered that some other effects must account for the discrepancies seen in the comparisons between the linear model and ROMS velocity data.

4.2 Linear shallow-water theory performance

Results for the basins of the Nordic Seas show that linear shallow-water theory, with only the surface- and bottom stress as inputs, is sufficient to closely capture the behaviour of a complex ocean model (see figures 3.2 and 3.4). This is true on time scales of ten days to about a year, according to the coherence plots of figure 3.10. However, the average velocity plots for the basins suggest that the solutions follow each other closely for the whole time series of five years.

Common for these basins is that they are mostly ice-free and the wind stress is cyclonic on average. Correlations for the Nordic Seas are 0.893 in the Norwegian Basin and 0.903 in the Greenland Basin. Regarding coherence, the results of this study are at comparable levels to those of Isachsen et al. (2003).

For the basins of the Arctic Ocean, the linear model struggles more to reproduce the results of ROMS data. The poorest results are those for the Makarov Basin, where, upon visual inspection of figure 3.7, it seems the linear model neither captures the variability nor the sign of the circulation found in the ROMS data, at least for the deepest contours. Of the three basins the Eurasian Basin has the best results, in particular when the surface stress is in a strong cyclonic period. In the Canadian Basin, which has anticyclonic motion on average, the linear model yields much too strong anticyclonic circulation values.

The coherence for the Eurasian Basin is at quite high values for most frequencies. It is not as high in the Canadian Basin, but still at levels that suggest a clear connection between the two models' solutions, particularly for the lower frequencies. The above assessment of the Makarov Basin is reflected for the coherence. The correlations support these assessments, with very low values for the contours in the Makarov and deep Canadian Basins, and comparably higher for the Eurasian and shallow Canadian Basins.

The overall impression from the results is that the linear model performs well, compared to the ROMS model data, when it produces cyclonic flow. For anticyclonic motion it evidently struggles, amplifying its strength, as shown in the scatter plots of section 3.3.

As a measure of linear connection between two variables, high correlation is a promising indicator. However, the goal of this study is to find whether the linear model can be used as a representation for the actual circulation of ocean basins. Therefore, along with correlations, the slope of the scattered data is interesting. The scatter plots presented in section 3.3 show that there is no one-to-one correspondence on average between the linear model and ROMS data. A more thorough routine for selecting the best value for R could involve correlation as a first check, then viewing the slope of the scatter plots where the linear model yields cyclonic data. The R-value that yields the slope closest to 1:1, while the intercept is close to zero and scatter is slim, should be chosen. The reason why only the cyclonic data should be viewed is due to the fact, mentioned above, that the linear model struggles to represent the anticyclonic motion

4.3 Prograde and retrograde flow asymmetry

The observed discrepancy between cyclonic (prograde) and anticyclonic (retrograde) motion was an unexpected result. Though, such asymmetry has already been described by others (Bretherton and Haidvogel, 1976, Carnevale and Frederiksen, 1987, for turbulent geophysical flow, and Nycander and LaCasce, 2004 specifically for seamounts).

For the steady state of a shallow-water framework on the f-plane LaCasce et al. (2008) found that, with a realistic representation of the Nordic Seas bathymetry, solutions for cyclonic motion follow the bathymetric contours, while anticyclonic

flow is characterised by extensive cross-isobath flow and eddy activity. This behaviour is attributed to standing topographic wave modes, that are not found in the linear scheme of this study. Here, time-varying flow is described, but the cyclonic and anticyclonic asymmetry is still prevalent. It is manifested in the ROMS velocity's unwillingness to respond linearly to negative surface stress, and can be seen for all basins. In the predominantly cyclonic motion of the Nordic Seas basins, the linear model produced values below those of the ROMS model's local minima, that are mostly cyclonic, shown in e.g. figures 3.2e and 3.4d. In those plots, the two data sets are quite equal for their maxima (equalling strong cyclonic motion), indicating that the bottom stress parameter is set at a reasonable value of 2.5×10^{-4} m/s.

For the steady state solutions of LaCasce et al. (2008), the retrograde case can be seen as an analogy to mountain waves, where a prograde mean-flow arrests the retrograde forced flow in spatially periodic streamlines that grow in amplitude. In the time-varying case the notion of a mean-flow is problematic. However, akin to the results of Carnevale and Frederiksen (1987), one can argue that the prograde case is nonlinearly stable, and the retrograde case is nonlinearly unstable. In any case, retrograde flow follows longer streamlines about the contour, than prograde flow.

A clear example of the asymmetry is found in the deepest contour, number 0, of the Eurasian Basin (figure 3.6a). At approximately day 1500 the linear model predicts the circulation to transition to anticyclonic, while the ROMS data stays cyclonic. On average, some of the contours of the Eurasian Basin have anticyclonic surface forcing, but none develop lasting anticyclonic circulation in the ROMS data. One of the conclusions of LaCasce et al. (2008) was that random fluctuations would develop cyclonic flow in basins, which agrees well with the results for the Eurasian Basin. Here, the results suggest that one can take the claim a step further, in that even an average anticyclonic surface forcing can support lasting cyclonic flow.

The Canadian Basin has anticyclonic flow, though the linear model exaggerates this circulation. This, again, reflects the systemic unwillingness to force anticyclonic motion. The poor results for the Makarov basin could potentially be amended by implementing the asymmetry in some manner.

Adaptive bottom stress parameter

A "quick-fix" for the challenge of the asymmetry could be to let R depend on the velocity. The bottom stress parameter is a simplification, and the usual expression for bottom stress, $\boldsymbol{\tau}_b = \rho C_D \boldsymbol{u}_b^2$, will in the shallow-water case include the velocity as $\boldsymbol{u}_b = \boldsymbol{u}$ (or $\boldsymbol{u}_b = \lambda \boldsymbol{u}$ [Isachsen et al., 2003] in an analytical equivalent barotropic case). In the expression, C_D is the drag coefficient and the subscript denotes **b**ottom.

The point of using the R-parameterisation is to obtain a linear equation, so having an $R = R(\boldsymbol{u})$ defeats this point. However, the implementation could be done in such a way that R has one value for positive velocities, and another for negative velocities. A longer streamline for the flow to follow, results in more stress acted upon it, such that the effective bottom stress for retrograde flows is larger than for prograde flows. This approach could work well in cases

where the goal is to limit the strength of anticyclonic flow in the linear model, e.g. in the Canadian Basin. However, it does not deter the flow of the linear model to transfer from cyclonic to anticyclonic. Neither does it address the cases where the linear model exaggerates the cyclonic minima that the ROMS model produces in the Nordic Seas.

As the oceanic response to surface forcing is quite immediate, shown in figure 3.14, for instance, letting the bottom friction parameter depend on the surface stress could be considered legitimate. With this approach, one could let R decrease for weak cyclonic and all anticyclonic surface forcing in the cyclonic flow case. This reduction of friction would halt the deceleration of the flow, effectively postponing its transition to an anticyclonic state or shifting a cyclonic minimum to higher values. Such a measure could perhaps increase the skill for results in the Nordic Seas and Eurasian Basin. For the anticyclonic circulation case, R should be increased whatever the sign or magnitude of the forcing is. Potentially, R could increase with the magnitude of $\boldsymbol{\tau}$ for negative (anticyclonic) forcing, to prevent the linear model from diverging strongly from the ROMS model circulation, as seen at around day 800 in figure 3.9, while not confining the flow too close to zero.

Implementing a heavily engineered bottom stress parameter in the linear model, could increase the skill, but would complicate it significantly. This goes against the primary motivation of the thesis, stated in the first section of chapter 1, in that complexity can reduce intuitive understanding. Also, having the bottom stress depend only on the surface stress is somewhat unphysical, as it is the oceanic velocity, along with the bottom roughness, that establishes the actual bottom stress.

4.4 Lateral vorticity fluxes

As mentioned in section 4.1, the inclusion of eddy lateral vorticity fluxes, does not contribute to improve circulation results. Viewing the vorticity flux contributions described in section 3.4, it is evident that these are large for the deepest contours (exemplified by figure 3.13 for contour 2, in the Norwegian Basin). The along-contour velocities are weak, and thus the eddy vorticity activity can dictate some of the flow. This is reflected in the relatively poor correlations for the deepest contours of the Norwegian an Greenland Basins seen in the corresponding tables of section 3.1. The linear model proved to work well for the shallower contours, with stronger cyclonic forcing and response. An interesting observation for the vorticity fluxes is that their contribution to the circulation is at the same quantitative scale for all contours. Thus, it seems the chaotic small- to mesoscale eddy activity is quite homogeneous, at least in the ROMS model.

This result could indicate at which average velocities the linear theory is valid. The velocities of contour 2 in figure 3.2a, could roughly define this velocity range. This contour has model velocities of about $0.5-2.5$ cm/s, which suggests that the linear model should be sufficient for velocities larger than that, or conversely, that lateral vorticity fluxes are negligible in flow faster than this.

4.5 Effects of stratification

The shallow-water approach of this study disregards any density stratification of the ocean. In the Nordic Seas there is weak stratification, and this study shows that shallow-water theory can reproduce the motion for the basins there. The Arctic Ocean has a significant vertical density gradient, due to fresher water high in the column, which could potentially have the ocean respond differently to the surface stress. This could happen through the deformation of the interface between density layers due to Ekman pumping or suction. With cyclonic flow, the surface Ekman transport moves water away from the basin, which is then balanced at depth with an inflow. Within the gyre, the water rises from depth and pushes the isopycnals upwards. The effect of baroclinicity is weakened flow at depth. Lower bottom velocity means that the depth-averaged velocity cannot be used in the bottom friction term, and the theory must be altered. However, baroclinic effects work on long time scales, and the rapidly varying surface stress fields sets up barotropic responses in the ocean that baroclinicity cannot respond to. These responses are effectively the same as those produced by shallow-water theory.

This consideration is supported in Isachsen et al. (2003). In their baroclinic examinations, the contribution from JEBAR (Joint Effect of Baroclinicity And Relief), was minimal in an integral balance term comparison, akin to those in section 3.4 for this study.

4.6 Advantages of different data

Observational data for the Arctic Region, and particularly the oceans of the region, is scarce. Satellite data is limited to the latitudes south of approximately 80°N, and measurements further north only cover transects or single points. As models are not a perfect representation of the system, the value of actual observations should not be understated. Meneghello et al. (2018) present observational data for the Canadian Basin that has permanent anticyclonic geostrophic surface currents due to surface Ekman stress. Although this motion is not the same as depth-averaged velocities, the result indicates that also observational data has anticyclonic motion for the Canadian Basin. Another interesting find in their study is that fast sea-ice decelerates the flow in wintertime. For regions covered by fast ice, the ocean is driven only by it's own inertia and, potentially, baroclinic effects. LaCasce et al. (2008) found that with a finite resolution model, there is always a stable anticyclonic mode along each closed f/H-contour, due to unresolved standing waves, that is not found in the real world. As the results of this thesis have consistent anticyclonic behaviour in the Canadian Basin, velocity measurements of the basin would be valuable to assess whether this is correctly captured in the ROMS model data.

On the other hand, exclusively working with model data ensures that the system has a closed budget, and thus that all information is available. Within the *model reality*, all mechanisms are accounted for, and the data coverage is constant throughout domain. Therefore, models are beneficial for studies such as this, particularly as the observational base is comparatively sparse. An ideal method to perform this study would be, as a final step, to compare the results to observations for verification.

4.7 Model resolution considerations

As mentioned in section 1.2, Isachsen et al. (2003) used a model with spatial and temporal resolutions of $O(100)$ km and one month, which is much too large to resolve eddy activity. With this model, they obtained very good results for the circulation in the Canadian Basin, when forcing it with ice-velocities. The surface forcing came from a reanalysis, so the surface winds were anticyclonic on average, due to the Beaufort high.

The prograde and retrograde flow asymmetry can only exist in an eddy-resolving environment. Thus, the results of this study suggests that the results for the Canadian Basin in Isachsen et al. (2003) are probably artificially good, due to the asymmetry not being present. A coarse model effectively linearises the dynamics, due to the lack of eddies - and parameterises eddies as diffusion of kinetic energy. Therefore it is as expected that the circulation results from a linear equation correspond well with model circulation. This claim is not completely satisfying, however, because the results of Isachsen et al. (2003) for the Eurasian Basin are poor compared to those in the Canadian Basin. This basin is also largely ice-covered year-round. As they were trying to mimic a coarse resolution model, it does remain a mystery why it worked for one ice-covered basin, and not another. They concluded that it could be due to some error in the surface stress parameterisation and that dense-water inflow from the Barents Sea could affect the result. Note that, in their study, the results presented for the model comparison are displayed in terms of coherence.

In this thesis, the results for the Eurasian Basin are much better, even with resolved eddy flow fields, and only top and bottom stress as inputs. Though, this still does not give any obvious hints as to why the calculations of Isachsen et al. (2003) yielded such poor results, but the intrusion of Barents Sea water seems to not be a crucial factor.

Other considerations regarding model resolutions for this study include the definition of "large-scale" and the optimal smoothing of bathymetry. Here, the bathymetry was smoothed by a filter of about 40 km, which was quite an ad hoc choice. Though, it was made sure that the mesoscale variations were filtered out, but no debate on an optimal smoothing resolution was performed. Another brief point to make, is that the coherence plots of section 3.2 are quite noisy for the shortest time scales, between 2 and 10 days approximately. This can most likely be attributed to eddy activity. The corresponding plots in Isachsen et al. (2003) go from time scales of 2 months to 5 years, and at these scales any noise is smoothed out.

4.8 Future outlook for the study region

Predictions for Arctic sea-ice in the coming decades propose a complete disappearance of multi-year ice, having no sea-ice in summer (Haine and Martin, 2017). This future Arctic would have much thinner, and more mobile ice. Hypothetically, the surface stress on the Arctic Ocean could increase in intensity (a decrease in surface roughness could have the opposite contribution). As the mean momentum transfer to the ocean is anticyclonic there is, however, no clear indication that bathymetry-following (or f/H-following) circulation would

increase in intensity. Following the arguments of LaCasce et al. (2008), increased anticyclonic forcing would increase the eddy activity in the region. Particularly the Eurasian basin - which has cyclonic flow in the results of this study, but net anticyclonic forcing - could experience weakened flow or potentially switch to anticyclonic flow. The Canadian Basin could respond to stronger forcing, with a slightly stronger anticyclonic motion. Though, much of the energy would dissipate in chaotic small scale flows, again due to the prograde and retrograde asymmetry.

As the coupled atmosphere-ocean system works both ways, a change in the ocean would induce change in the atmosphere dynamics as well. Kenigson and Timmermans (2021) found signs of an increasing amount of Arctic cyclones, with a corresponding weakening of the Beaufort high. This result effectively predicts stronger cyclonic forcing of the region in the future. However, one effect of diminishing sea-ice is a greater oceanic heat-loss to the atmosphere, which increases the atmospheric pressure. Such an effect would suggest a stronger Beaufort high. It is, therefore, difficult to give a precise prognosis for the future state of the Arctic, at least in terms of dynamics.

The joint effects of a more energetic atmosphere, but weaker South-North temperature gradient due to Arctic amplification, hinder a straightforward prognosis for circulation of the Nordic Seas as well. An increase of atmospheric energy translates to, among other effects, stronger winds. Storms regularly advect into the Nordic Seas from the South-West, and accelerate the circulation in the Norwegian and Greenland Basins. One could imagine that stronger storms would strengthen the circulation further. However, it is projected that storms will appear in this region more infrequently in the future climate (Tunes, 2021). This change would let the bottom friction dampen the flow for longer periods in between storms. As such, it is difficult to say whether the mean circulation changes at all, or if it is strengthened or weakened, in the future. Note that the circulation will continue to be cyclonic for the basins, and that not only storms drive the ocean. The oceanic activity in the Nordic Seas can be felt in the Arctic as well, due to f/H-contours that encompass both regions. The adverse is also true, that the Nordic Seas can feel the forcing of the Arctic Ocean.

CHAPTER 5

Conclusion

This study shows that a simple linear model derived from shallow-water equations can capture the dynamics of closed f/H-contours as represented in a complex high-resolution ocean model. It is further experienced that the linear model lacks the mechanisms and complexity to describe the evident asymmetry in prograde and retrograde flows. Some suggestions on how to parameterise this asymmetry are given, but it is noted that increasing the complexity of the linear model is contradictory to the motivation of simplicity improving intuition. The inclusion of eddy lateral vorticity fluxes yielded no apparent improvement in the performance of the theory, but it highlighted the minimum velocity values, below which the output from the linear model is not trustworthy. At these lower velocities, the velocity contribution from eddy activity is of the same scale the surface stress contribution.

Any future work within this theory framework should use the f-plane approximation, as the linear model expression is mathematically inconsistent. It is also noted that the inclusion of observations as a final step in the analysis, could aid in verification of both models' output. One could also explore different ways to implement the above mentioned asymmetry, and perhaps involve more tests than correlation to obtain an optimal value for R.

The final discussion point was that the future state of the study region is highly uncertain, with different mechanisms counteracting, or working in tandem to drive the system. This result provides motivation to perform more targeted studies, such as this one. Isolating a few variables, and analysing their effect, is a way forward to obtain crucial intuitive knowledge about the climate system.

APPENDIX A

Computer code and data

The following link contains all code written for this study, along with all figures that were made. https://github.com/magnudry/Master-deg.git

Bibliography

Boers, N. (2021). 'Observation-based early-warning signals for a collapse of the Atlantic Meridional Overturning Circulation'. In: *Nature Climate Change* vol. 11.

Brayshaw, D. J., Hoskins, B. and Blackburn, M. (2011). 'The Basic Ingredients of the North Atlantic Storm Track. Part II: Sea Surface Temperatures'. In: *Journal of the Atmospheric Sciences* vol. 68, pp. 1784–1805.

Bretherton, F. P. and Haidvogel, D. B. (1976). 'Two-dimensional turbulence above topography'. In: *Journal of Fluid Mechanics* vol. 78, no. 1, pp. 129–154.

Carnevale, G. F. and Frederiksen, J. S. (1987). 'Nonlinear stability and statistical mechanics of flow over topography'. In: *Journal of Fluid Mechanics* vol. 175, pp. 157–181.

Eyring, V., Bony, S., Meehl, G. A., Senior, C. A., Stevens, B., Stouffer, R. J. and Taylor, K. E. (2016). 'Overview of the Coupled Model Intercomparison Project Phase 6 (CMIP6) experimental design and organization'. In: *Geoscientific Model Development* vol. 9, pp. 1937–1958.

Haine, T. W. N. and Martin, T. (2017). 'The Arctic-Subarctic sea ice system is entering a seasonal regime: Implications for future Arctic amplification'. In: *Scientific Reports* vol. 7.

Helland-Hansen, B. and Nansen, F. (1909). *The Norwegian sea : its physical oceanography based upon Norwegian researches 1900-1904*. Vol. 2. Report on Norwegian fishery and marine investigations 2. Det Mallingske bogtrykkeri.

Isachsen, P. E., LaCasce, J. H., Mauritzen, C. and Häkkinen, S. (2003). 'Wind-Driven Variability of the Large-Scale Recirculating Flow in the Nordic Seas and Arctic Ocean'. In: *Journal of Physical Oceanography* vol. 33, pp. 2534–2550.

Kenigson, J. S. and Timmermans, M.-L. (2021). 'Arctic Cyclone Activity and the Beaufort High'. In: *Journal of Climate* vol. 34, pp. 4119–4127.

LaCasce, J. H., Nøst, O. A. and Isachsen, P. E. (2008). 'Asymmetry of Free Circulations in Closed Ocean Gyres'. In: *Journal of Physical Oceanography* vol. 38, pp. 517–526.

Meneghello, G., Marshall, J., Timmermans, M.-L. and Scott, J. (2018). 'Observations of Seasonal Upwelling and Downwelling in the Beaufort Sea Mediated by Sea Ice'. In: *Journal of Physical Oceanography* vol. 48, pp. 795–805.

Nycander, J. and LaCasce, J. H. (2004). 'Stable and unstable vortices attached to seamounts'. In: *Journal of Fluid Mechanics* vol. 507, pp. 71–94.

Previdi, M., Smith, K. L. and Polvani, L. M. (2021). 'Arctic amplification of climate change: a review of underlying mechanisms'. In: *Environmental Research Letters* vol. 16.

Serreze, M. C. and Barrett, A. P. (2011). 'Characteristics of the Beaufort Sea High'. In: *Journal of Climate* vol. 24, pp. 159–182.

Stroeve, J. C., Serreze, M. C., Holland, M. M., Kay, J. E., Malanik, J. and Barrett, A. P. (2011). 'The arctic's rapidly shrinking sea ice cover: a research synthesis'. In: *Climatic Change*.

Timmermans, M.-L. and Marshall, J. (2020). 'Understanding Arctic Ocean Circulation: A Review of Ocean Dynamics in a Changing Climate'. In: *Journal of Geophysical Research: Oceans* vol. 125.

Tunes, S. M. (2021). 'Changes in Cyclone Characteristics over the North Atlantic in the Norwegian Earth System Model'. Master's thesis. University of Oslo.

Aagard, K., Foldvik, A. and Hillman, S. R. (1987). 'The West Spitsbergen Current: Disposition and Water Mass Transformation'. In: *Journal of Geophysical Research* vol. 92, pp. 3778–3784.